RESEARCH ARTICLE OPEN ACCESS

# [$^{18}$F]Flortaucipir PET Across Various *MAPT* Mutations in Presymptomatic and Symptomatic Carriers

Emma E. Wolters, MD, PhD, Janne M. Papma, PhD, Sander C.J. Verfaillie, PhD, Denise Visser, MSc, Emma Weltings, MSc, Colin Groot, PhD, Emma L. van der Ende, MD, Lucia A.A. Giannini, MD, Hayel Tuncel, MSc, Tessa Timmers, MD, PhD, Ronald Boellaard, PhD, Maqsood Yaqub, PhD, Danielle M.E. van Assema, MD, PhD, Dennis A. Kuijper, MSc, Marcel Segbers, MSc, Annemieke J.M. Rozemuller, MD, PhD, Frederik Barkhof, MD, PhD, Albert D. Windhorst, PhD, Wiesje M. van der Flier, PhD, Yolande A.L. Pijnenburg, MD, PhD, Philip Scheltens, MD, PhD, Bart N.M. van Berckel, MD, PhD, John C. van Swieten, MD, PhD, Rik Ossenkoppele, PhD, and Harro Seelaar, MD, PhD

**Correspondence**
Dr. Wolters
e.e.wolters-2@umcutrecht.nl

*Neurology*® 2021;97:e1017-e1030. doi:10.1212/WNL.0000000000012448

## Abstract

### Objective

To assess the [$^{18}$F]flortaucipir binding distribution across *MAPT* mutations in presymptomatic and symptomatic carriers.

### Methods

We compared regional [$^{18}$F]flortaucipir binding potential ($BP_{ND}$) derived from a 130-minute dynamic [$^{18}$F]flortaucipir PET scan in 9 (pre)symptomatic *MAPT* mutation carriers (4 with P301L [1 symptomatic], 2 with R406W [1 symptomatic], 1 presymptomatic L315R, 1 presymptomatic S320F, and 1 symptomatic G272V carrier) with 30 cognitively normal controls and 52 patients with Alzheimer disease.

### Results

[$^{18}$F]Flortaucipir $BP_{ND}$ images showed overall highest binding in the symptomatic carriers. This was most pronounced in the symptomatic R406W carrier in whom tau binding exceeded the normal control range in the anterior cingulate cortex, insula, amygdala, temporal, parietal, and frontal lobe. Elevated medial temporal lobe $BP_{ND}$ was observed in a presymptomatic R406W carrier. The single symptomatic carrier and 1 of the 3 presymptomatic P301L carriers showed elevated [$^{18}$F]flortaucipir $BP_{ND}$ in the insula, parietal, and frontal lobe compared to controls. The symptomatic G272V carrier exhibited a widespread elevated cortical $BP_{ND}$, with at neuropathologic examination a combination of 3R pathology and encephalitis. The L315R presymptomatic mutation carrier showed higher frontal $BP_{ND}$ compared to controls. The $BP_{ND}$ values of the S320F presymptomatic mutation carrier fell within the range of controls.

### Conclusion

Presymptomatic *MAPT* mutation carriers already showed subtle elevated tau binding, whereas symptomatic *MAPT* mutation carriers showed a more marked increase in [$^{18}$F]flortaucipir $BP_{ND}$. Tau deposition was most pronounced in R406W *MAPT* (pre)symptomatic mutation carriers, which is associated with both 3R and 4R tau accumulation. Thus, [$^{18}$F]flortaucipir may serve as an early biomarker for *MAPT* mutation carriers in mutations that cause 3R/4R tauopathies.

From the Department of Radiology & Nuclear Medicine (E.E.W., S.C.J.V., D.V., E.W., H.T., T.T., R.B., M.Y., F.B., A.D.W., B.N.M.v.B.) and Alzheimer Center Amsterdam, Department of Neurology (E.E.W., C.G., W.M.v.d.F., Y.A.L.P., P.S., R.O.), Amsterdam Neuroscience, and Department of Epidemiology and Biostatistics (W.M.v.d.F.), Vrije Universiteit Amsterdam, Amsterdam UMC; Department of Neurology, Alzheimer Center (J.M.P., E.L.v.d.E., L.A.A.G., J.C.v.S., H.S.), and Department of Radiology & Nuclear Medicine (D.M.E.v.A., D.A.K., M.S.), Erasmus MC University Medical Center, Rotterdam; Department of Pathology (A.J.M.R.), Amsterdam Neuroscience, Amsterdam UMC, location VUmc, the Netherlands; Institutes of Neurology & Healthcare Engineering (F.B.), UCL, London, UK; and Clinical Memory Research Unit (R.O.), Lund University, Sweden.

Go to Neurology.org/N for full disclosures. Funding information and disclosures deemed relevant by the authors, if any, are provided at the end of the article.

The Article Processing Charge was funded by the authors.

This is an open access article distributed under the terms of the Creative Commons Attribution-NonCommercial-NoDerivatives License 4.0 (CC BY-NC-ND), which permits downloading and sharing the work provided it is properly cited. The work cannot be changed in any way or used commercially without permission from the journal.

Copyright © 2021 The Author(s). Published by Wolters Kluwer Health, Inc. on behalf of the American Academy of Neurology.

## Glossary

**ACC** = anterior cingulate cortex; **AD** = Alzheimer disease; **$BP_{ND}$** = [$^{18}$F]flortaucipir binding potential; **bvFTD** = behavioral variant frontotemporal dementia; **CDR** = Clinical Dementia Rating; **FTD** = frontotemporal dementia; **MMSE** = Mini-Mental State Examination; **NACC-FTLD** = National Alzheimer's Coordinating Center–Frontotemporal Lobar Degeneration; **PHF** = paired helical filament; **rCBF** = relative cerebral blood flow; **RPM** = receptor parametric mapping; **SUVr** = standardized uptake value ratio; **VOI** = volume of interest.

Frontotemporal dementia (FTD) is a clinically and pathologically heterogeneous neurodegenerative disorder characterized by behavioral changes[1] or language difficulties.[2] Mutations in the micro-tubule-associated protein tau gene (*MAPT*) are a frequent cause of familial FTD. Alternative mRNA splicing from the *MAPT* gene produces 6 different tau isoforms, including 3 (3R, 3 isoforms) and 4 (4R, 3 isoforms) repeat tau, which are found in equal amounts in the normal adult brain. Mutations in the *MAPT* gene may affect the normal function of the tau protein (exons 9–13) or alter the balance between 3R and 4R (exon 10). Therefore, exon 10 mutations like P301L typically lead to an abundance of 4R tau. Mutations outside exon 10 usually affect all isoforms, with most *MAPT* mutations resulting in a combined 3R/4R tauopathy (e.g., L315R, S320F). This sometimes results in 3R/4R paired helical filaments (PHFs) of tau comparable to Alzheimer disease (AD) tauopathy (e.g., in R406W), while other mutations (e.g., G272V) lead to an increased aggregation of 3R tau only.[3] Imaging biomarkers could help to assess the regional distribution of tau pathology in (pre)symptomatic *MAPT* mutation carriers years before symptom onset.

[$^{18}$F]Flortaucipir is a PET tracer with high affinity to tau aggregates, offering the opportunity to examine the heterogeneity of tau pathology observed in *MAPT* mutation carriers. [$^{18}$F]Flortaucipir binds with high affinity to PHFs in AD.[4,5] Previous studies of [$^{18}$F]flortaucipir in *MAPT* mutation carriers have shown frontal and temporal tau PET uptake primarily in combined 3R/4R tau pathology, but not exclusively.[6-12] Few [$^{18}$F]flortaucipir studies have included presymptomatic *MAPT* carriers[8,13] and showed elevated as well as negligible cortical tau pathology. The identification of appropriate biomarkers to detect FTD prior to symptom onset is crucial and could advance the development of disease-modifying drugs and evaluation of early intervention. Therefore, the aim of this study was to use [$^{18}$F]flortaucipir PET to assess regional distribution of tau across *MAPT* mutations in presymptomatic and symptomatic carriers.

## Methods

### Recruitment of Participants

Patients with 50% risk of developing familial FTD were recruited from Dutch families with *MAPT* mutations from the FTD-RisC study, as previously described.[14] Briefly, as part of the FTD-RisC study, all participants underwent annual or biannual follow-up standardized clinical assessment, including neuropsychological testing and brain MRI.[14,15] All participants with a possible *MAPT* mutation were considered except for those who met exclusion criteria: (1) significant cerebrovascular disease on MRI (e.g., territorial infarct); (2) major traumatic brain injury; (3) major psychiatric or neurologic disorders other than behavioral variant FTD (bvFTD); (4) current substance abuse. We included a total of 13 participants; DNA genotyping revealed 9 *MAPT* mutation carriers and 4 noncarriers (healthy controls from a *MAPT* mutation family). The clinical investigators (H.S., J.C.v.S.) and participants were blinded for the participants' genetic status, except for those who underwent predictive testing at their own request. For confidentiality reasons, sex is not provided, and age range is provided in Table 1.

Here we only report on the *MAPT* mutation carriers, including 6 presymptomatic and 3 symptomatic carriers. All symptomatic and 5 presymptomatic carriers were aware of their mutation status. All symptomatic mutation carriers met diagnostic criteria for bvFTD,[1] and other clinical phenotypes (i.e., primary progressive aphasia) were not observed in symptomatic carriers. Diagnostic criteria were supported by extensive neuropsychological assessment, behavioral testing, and supportive neuroimaging findings, after a multidisciplinary consensus meeting of the Erasmus University Medical Center. Mutation carriers were considered presymptomatic when diagnostic criteria for bvFTD[1] were not met. We classified mutation carriers as converters if they met the following criteria: (1) progressive deterioration of behavior or language by observation or history (as provided by a knowledgeable informant); (2) significant functional decline (evidenced by increased Clinical Dementia Rating (CDR) plus National Alzheimer's Coordinating Center–Frontotemporal Lobar Degeneration (NACC-FTLD) sum of boxes scores at the first or second follow-up visit and CDR plus NACC-FTLD score ≥1); and (3) cognitive deficits in at least one domain of the neuropsychological assessment. Neuropsychological assessment covered the following cognitive domains: language, processing speed, executive functioning, memory, social cognition, visuoconstructive ability, and orientation, as described before[15] (for separate neuropsychological tests, see eTable1, data available from Dryad, doi.org/10.5061/dryad.3tx95x6g1). We report the Mini-Mental State Examination (MMSE), Frontal Assessment Battery, CDR plus NACC-FTLD, and CDR plus NACC-FTLD sum of boxes. Symptomatic *MAPT* mutations included P301L (n = 1), R406W (n = 1), and G272V (n = 1). Presymptomatic *MAPT* mutations included P301L (n = 3), R406W (n = 1), L315R (n = 1), and

**Table 1** Overview of *MAPT* Mutation Carrier Characteristics

| Case | Age range, y | *MAPT* mutation | Clinical diagnosis | MMSE on day of PET |
|---|---|---|---|---|
| **1** | 50–60 | P301L | bvFTD | 8 |
| **2** | 30–40 | P301L | Presymptomatic | 25 |
| **3** | 40–50 | P301L | Presymptomatic | 29 |
| **4** | 40–50 | P301L | Presymptomatic | 30 |
| **5** | 40–50 | R406W | bvFTD | 23 |
| **6** | 40–50 | R406W | Presymptomatic | 30 |
| **7** | 40–50 | S320F | Presymptomatic | 29 |
| **8** | 70–80 | L315R | Presymptomatic | 28 |
| **9** | 40–50 | G272V | bvFTD | 28 |

Abbreviations: bvFTD = behavioral variant frontotemporal dementia; MMSE = Mini-Mental State Examination.

S320F (n = 1). We grouped mutation carriers based on their coding exon, expected tau isoforms, and number of carriers within the *MAPT* mutation. First, we present P301L mutations, involving exon 10, which mainly is associated with the 4R isoform of tau. Second, we present exon 13 R406W mutation carriers, which tend to form both 3R and 4R tau pathology, comparable to AD. Third, we present presymptomatic *MAPT* mutation carriers of exon 11 (L315R and S320F), which tend to form 3R/4R. Finally, we present a *MAPT* mutation exon 9 carrier (G272V), which is composed of 3R tau.

In addition, to assess whether tau PET binding of *MAPT* mutation carriers deviates from the distribution of cognitively normal controls and of patients with AD, we included 2 reference groups that were previously described in greater detail.[16] First, we included 30 cognitively normal controls (66 ± 8 years, 50% female, MMSE 29 ± 1) of the SCIENCe study.[17] Second, we included 52 participants diagnosed with AD (66 ± 8 years, 48% female, MMSE 23 ± 3), who met core clinical criteria according to the National Institute on Aging and Alzheimer's Association. All controls were amyloid-negative and all patients with AD were amyloid-positive based on visual assessment of [$^{18}$F]florbetapir PET scans or CSF biomarkers.[16]

## Imaging and Processing

All *MAPT* mutation carriers underwent a single dynamic 130-minute [$^{18}$F]flortaucipir PET scan on a Siemens Biograph mCT PET/CT. The scanning protocol consisted of 2 dynamic PET scans of 60 and 50 minutes, respectively, with a 20-minute break in between.[16] The first 60-minute dynamic acquisition started simultaneously with a bolus injection 229 ± 7 MBq [$^{18}$F]flortaucipir (injected mass 1.26 ± 0.47 μg, details for *MAPT* mutation carriers). PET list mode data were rebinned into a total of 29 frames and were reconstructed using an OSEM 3D time-of-flight enabled iterative reconstruction (4i21s) with a matrix size of 400 × 400 × 111 and a final voxel size of 2.036 × 2.036 × 2.0 mm$^3$, including standard corrections for dead time, decay, attenuation, randoms, and scatter. Each PET dataset consisted of 29 frames in total; the last 10 frames stemmed from the second PET scan session. The second 50-minute PET acquisition was coregistered to the first dynamic PET scan using Vinci software. Finally, PET scans from the Siemens scanner were in addition smoothed using a Gaussian filter (4 mm full width at half maximum) in order to correspond to smoothing kernels of the SCIENCe and AD dataset (Philips Ingenuity TF PET/CT).

In addition, for gray matter segmentation purposes, all *MAPT* mutation carriers underwent a 3D T1-weighted sequence MRI scan on a Philips 3T Achieve MRI scanner using an 8-channel SENSE head coil. Except for the scanner type, details of [$^{18}$F]flortaucipir image and MRI acquisition of the SCIENCe and AD datasets are comparable and have been described elsewhere.[16]

We coregistered native 3D T1 MRI to the averaged images of frames 8–29 of the dynamic PET scan using Vinci software. We defined the volumes of interest (VOIs, including separate VOIs for left and right hemisphere) on MRI scans using PVElab according to the probabilistic Hammers brain atlas.[18] Time activity curves were generated and [$^{18}$F]flortaucipir binding potential ($BP_{ND}$) was extracted using receptor parametric mapping (RPM)[19] and standardized uptake*value*ratio (SUVr) images were generated for the time interval 80–100 minutes postinjection, while using cerebellar gray matter as a reference region. RPM also allows for the additional quantification of $R_1$ images. $R_1$ is a proxy for relative cerebral blood flow (rCBF)[20] and because hypoperfusion has been observed previously in (pre)symptomatic *MAPT* mutation carriers,[21,22] we investigated $R_1$ in a secondary analysis to assess the regional distribution of rCBF.

Methods of regional/voxelwise analysis are described in detail in eAppendix 1 (data available from Dryad, doi.org/10.5061/dryad.3tx95x6g1). In short, we created a priori 9 VOIs

**Figure 1** Voxel-Wise [$^{18}$F]Flortaucipir Parametric Binding Potential ($BP_{ND}$) Images, T1-Weighted MRI, and Regional [$^{18}$F] Flortaucipir $BP_{ND}$ Values of (Pre)symptomatic P301L Carriers; and (Pre)symptomatic P301L Mutation Carriers vs Controls and vs Patients With Alzheimer Disease (AD)

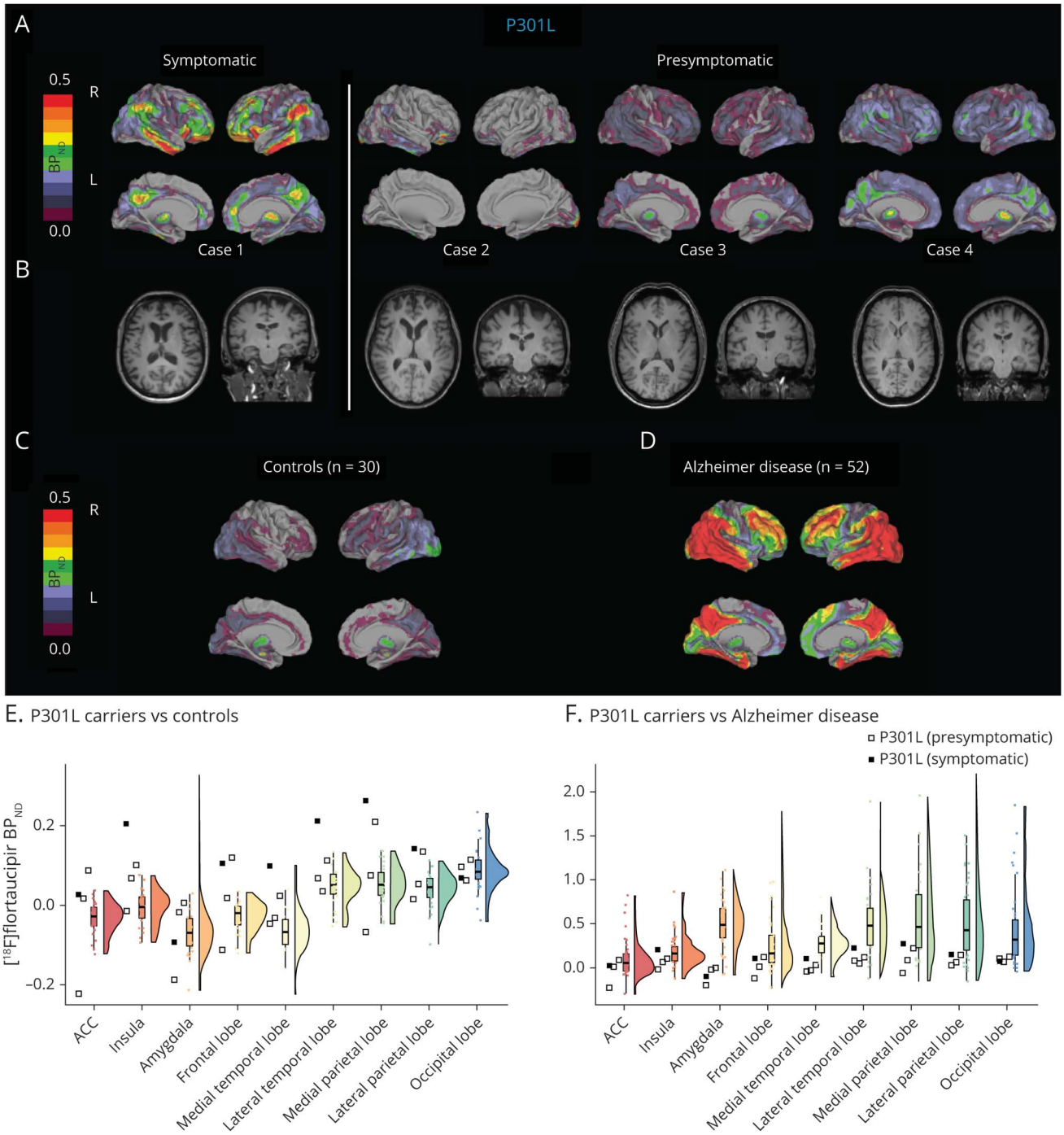


Voxel-wise [$^{18}$F]flortaucipir parametric $BP_{ND}$ images (A), T1-weighted MRI (B), and regional [$^{18}$F]flortaucipir $BP_{ND}$ (C, D) values of (pre)symptomatic P301L carriers. (E, F) (Pre)symptomatic P301L mutation carriers (displayed individually) vs controls (C, E) and vs patients with AD (D, F, both displayed as the average of the group). Open and closed squares depict presymptomatic and symptomatic P301L mutation carriers, respectively. The order of the presymptomatic cases is the same as the order of A and B (from left to right). ACC = anterior cingulate cortex.

(anterior cingulate cortex [ACC], insula, amygdala, frontal, medial/lateral temporal/parietal regions) and compared these regional $BP_{ND}/R_1$/SUVr values between *MAPT* mutation carriers and controls/AD. Analyses were performed using R (version 3.5.3, R Development Core Team 2019).

## Neuropathology

Neuropathology was available in one patient (symptomatic G272V carrier), who died aged 45, 10 months after the [$^{18}$F] flortaucipir PET. The Netherlands Brain Bank performed brain autopsy according to their Legal and Ethical Code of

Conduct. Tissue blocks were taken from the left hemisphere from all cortical lobe hippocampus (both left and right), amygdala, basal ganglia, substantia nigra, pons, medulla oblongata, cerebellum, and cervical spinal cord, and were embedded in paraffin blocks. Immunohistochemistry was performed as previously described.[22] In addition, immunochemical staining with AT-8 (Thermo Fisher Scientific, MN1020; dilution 1:200), RD3 (Millipore clone 8E6/C11, 05-803), RD4 (Millipore, clone 1E1/A6, 1:1,000), CD3 (DAKO, A0452, 1:150), and HLA-DR (DAKO, M0775, 1:100) antibodies were performed in a subset of slides. Silver staining using the Gallyas method was performed on hippocampal and temporal tissue sections.

### Standard Protocol Approvals, Registrations, and Patient Consents

All procedures were in accordance with the ethical standards of the Medical Ethics Review Committee of the Amsterdam UMC location VU Medical Center and the Erasmus University Medical Center according to the 1964 Helsinki declaration and its later amendments or comparable ethical standards. Written informed consent was obtained from all participants.

### Data Availability

Data not published within the article are available in a public repository and include digital object identifiers (doi.org/10.5061/dryad.3tx95x6g1). Anonymized data used in the present study may be available upon request to the corresponding author.

## Results

### Demographics

Demographic and clinical characteristics of the (pre)symptomatic *MAPT* mutation carriers are presented in Table 1. Further details of screening, behavioral, and neuropsychological test results are presented in eTable 1 (data available from Dryad, doi.org/10.5061/dryad.3tx95x6g1).

### (Pre)Symptomatic P301L Mutation Carriers

Figure 1 shows voxel-wise and regional [$^{18}$F]flortaucipir $BP_{ND}$ images/values and corresponding MRI of (pre)symptomatic P301L mutation carriers (Figure 1, A, B, E, F) vs controls (Figure 1, C and E) and patients with AD (Figure 1, D and F) as a reference group.

The symptomatic P301L carrier showed visually higher $BP_{ND}$ than the presymptomatic P301L cases, with highest $BP_{ND}$ in the orbitofrontal cortex, inferior temporal, and parietal lobe (Figure 1A). Regional [$^{18}$F]flortaucipir $BP_{ND}$ in the insula, frontal, medial/lateral temporal, and parietal lobe was higher than in controls (Figure 1E).

Presymptomatic P301L cases showed variable [$^{18}$F]flortaucipir $BP_{ND}$, ranging from minimal (case 2) to widespread tau higher binding in frontoparietal regions, including precuneus and posterior cingulate (case 3) (Figure 1A). All regional $BP_{ND}$ values of presymptomatic P301L case 2 and 3 fell within the distribution of controls. Presymptomatic P301L case 4 showed increased [$^{18}$F]flortaucipir $BP_{ND}$ in ACC, insula, frontal, and medial/lateral parietal lobe compared to the range of values in controls (Figure 1E), but within the range of patients with AD (Figure 1F).

### (Pre)Symptomatic R406W Mutation Carriers

Figures 2–4 show the voxel-wise [$^{18}$F]flortaucipir $BP_{ND}$ images (A) and regional [$^{18}$F]flortaucipir $BP_{ND}$ values (C, D) in (pre)symptomatic mutation carriers vs controls (C) and patients with AD (D) as a reference group. Voxel-wise images of control and AD reference groups are shown in Figure 1, C and D, respectively. The symptomatic R406W patients revealed higher $BP_{ND}$ than the presymptomatic R406W carrier, with highest tau binding in the medial temporal lobe, temporal pole, amygdala, and frontoparietal regions on voxel-wise [$^{18}$F]flortaucipir $BP_{ND}$ images (Figure 2A). Regionally, $BP_{ND}$ in ACC, insula, amygdala, frontal, medial/lateral temporal, and medial parietal lobe was elevated compared to the distribution of controls (Figure 2C), and equal to the AD range (Figure 2D).

The presymptomatic R406W carrier showed tau binding largely restricted to the medial temporal lobe. Regional values confirmed this observation with regional medial temporal tau values exceeding the range of controls. In addition, there was higher $BP_{ND}$ in the amygdala compared to the values observed in controls (Figure 2C). For both R406W carriers, regional $BP_{ND}$ fell within the AD range (Figure 2D).

### Presymptomatic S320F, L315R Mutation Carriers

Minimal $BP_{ND}$ was observed in presymptomatic carriers. Small areas of elevated [$^{18}$F]flortaucipir $BP_{ND}$ appeared in the orbitofrontal and parieto-occipital regions in the S320F mutation carrier (Figure 3A), although regional $BP_{ND}$ fell within range of controls and patients with AD. The L315R mutation carrier showed higher frontal $BP_{ND}$ compared to the distribution of controls (Figure 3C), but did not exceed the $BP_{ND}$ range in patients with AD (Figure 3D).

### Symptomatic G272V Carrier Including Clinical Presentation and Neuropathology

The symptomatic G272V carrier exhibited a widespread cortical higher tau binding, with increased $BP_{ND}$ values in the ACC, insula, frontal, and medial/lateral parietal lobe in the G272V mutation carrier, relatively sparing the temporal lobe (Figure 4A) compared to the distribution in controls. All regional [$^{18}$F]flortaucipir $BP_{ND}$ values fell within range of AD (Figure 4D).

At age 39 years, 4 years before the diagnosis of bvFTD, the mutation carrier had occasional word-finding problems and panic attacks.[15] Neuropsychological testing and structural MRI were normal and the patient had CDR plus NACC-FTLD score of 0.5 (≥1 is abnormal, i.e., symptomatic). At age

**Figure 2** Voxel-Wise [$^{18}$F]Flortaucipir Parametric Binding Potential ($BP_{ND}$) Images, T1 -Weighted MRI, and Regional [$^{18}$F] Flortaucipir $BP_{ND}$ Values of (Pre)symptomatic R406W Mutation Carriers; and (Pre)symptomatic R406W Mutation Carriers vs Controls and vs Patients With Alzheimer Disease (AD)

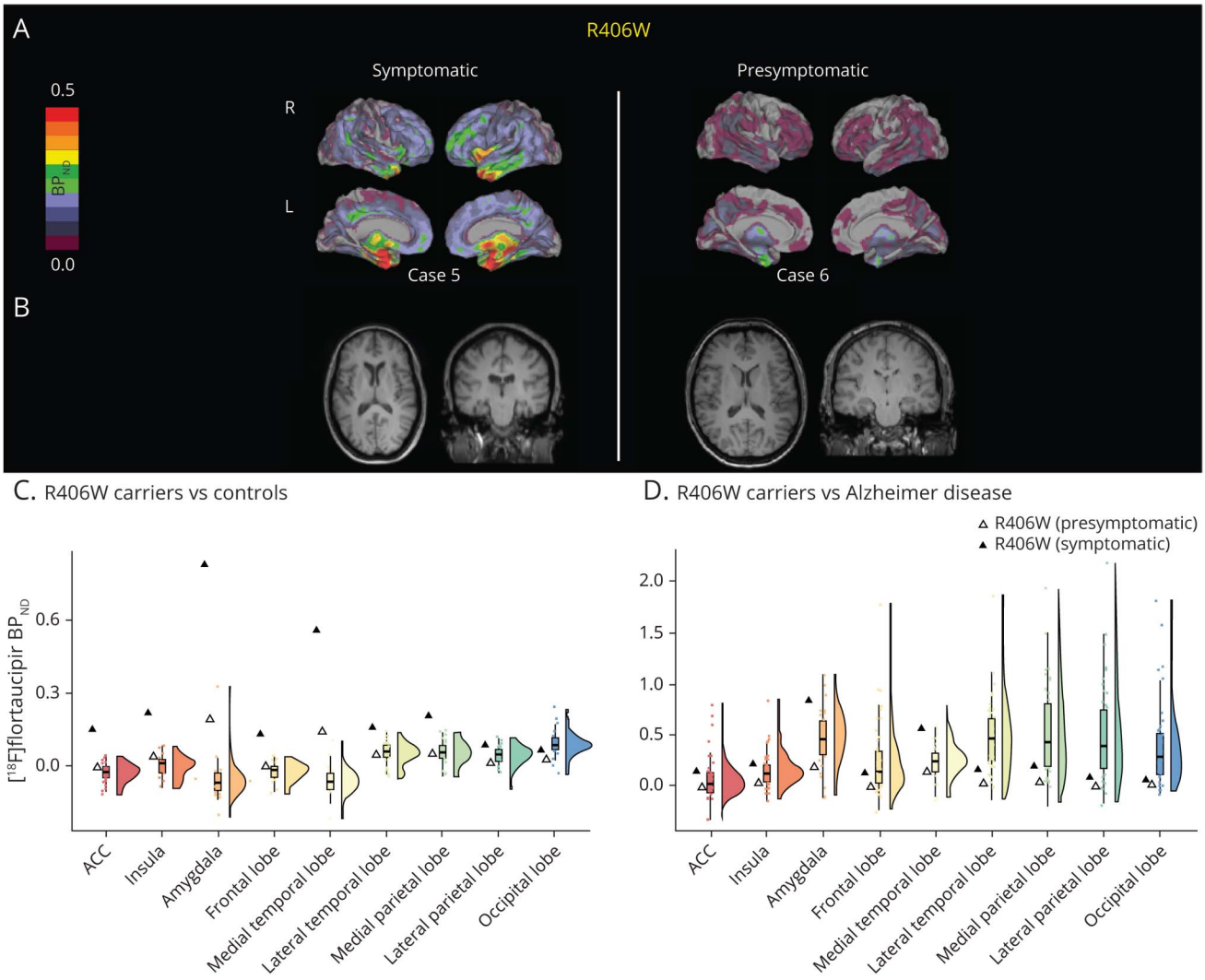


Voxel-wise [$^{18}$F]flortaucipir parametric $BP_{ND}$ images (A), T1-weighted MRI (B), and regional [$^{18}$F]flortaucipir $BP_{ND}$ (C, D) values of (pre)symptomatic R406W mutation carriers. (C, D) (Pre)symptomatic R406W mutation carriers (displayed individually) vs controls (C) and vs patients with AD (D, both displayed as the average of the group). Open and closed triangles depict presymptomatic and symptomatic R406W mutation carriers, respectively. ACC = anterior cingulate cortex.

41, the patient developed mild memory problems and semantic paraphasias in spontaneous speech, although neuropsychological and behavioral testing remained within normal limits. At age 42, the patient was unable to work due to difficulties with planning and remembering appointments, and complained about tiredness and depression. Six months before diagnosis, the patient was hospitalized for a manic episode after starting paroxetine for mood disturbances, which was quickly in remission after switching paroxetine to olanzapine and lorazepam. At age 43 years, the diagnostic criteria of bvFTD were met, supported by observations of word-finding difficulties, phonologic errors, and neuropsychological questionnaire results indicating mood problems, sleeping disturbances, euphoria, apathy, disinhibition, agitation, and aberrant motor behavior. Additional neuropsychological assessment showed deficits in episodic memory, mental speed, attention, and fluency, with CDR plus NACC-FTLD score of 1, and asymmetric, right-sided temporal atrophy was found on MRI.

One year postdiagnosis, the patient was unable to perform activities of daily living and attended day care 4 times a week. She died at age 45 years by euthanasia, 10 months after the [$^{18}$F]flortaucipir PET.

## Neuropathology

Brain section was carried out in the G272V patient. Macroscopically, there was very mild atrophy of the frontal lobes. The caudate nucleus was relatively small.

**Figure 3** Voxel-Wise [$^{18}$F]Flortaucipir Parametric Binding Potential ($BP_{ND}$) Images, T1 -Weighted MRI, and Regional [$^{18}$F] Flortaucipir $BP_{ND}$ Values of the Presymptomatic S320F, L315R Mutation Carriers

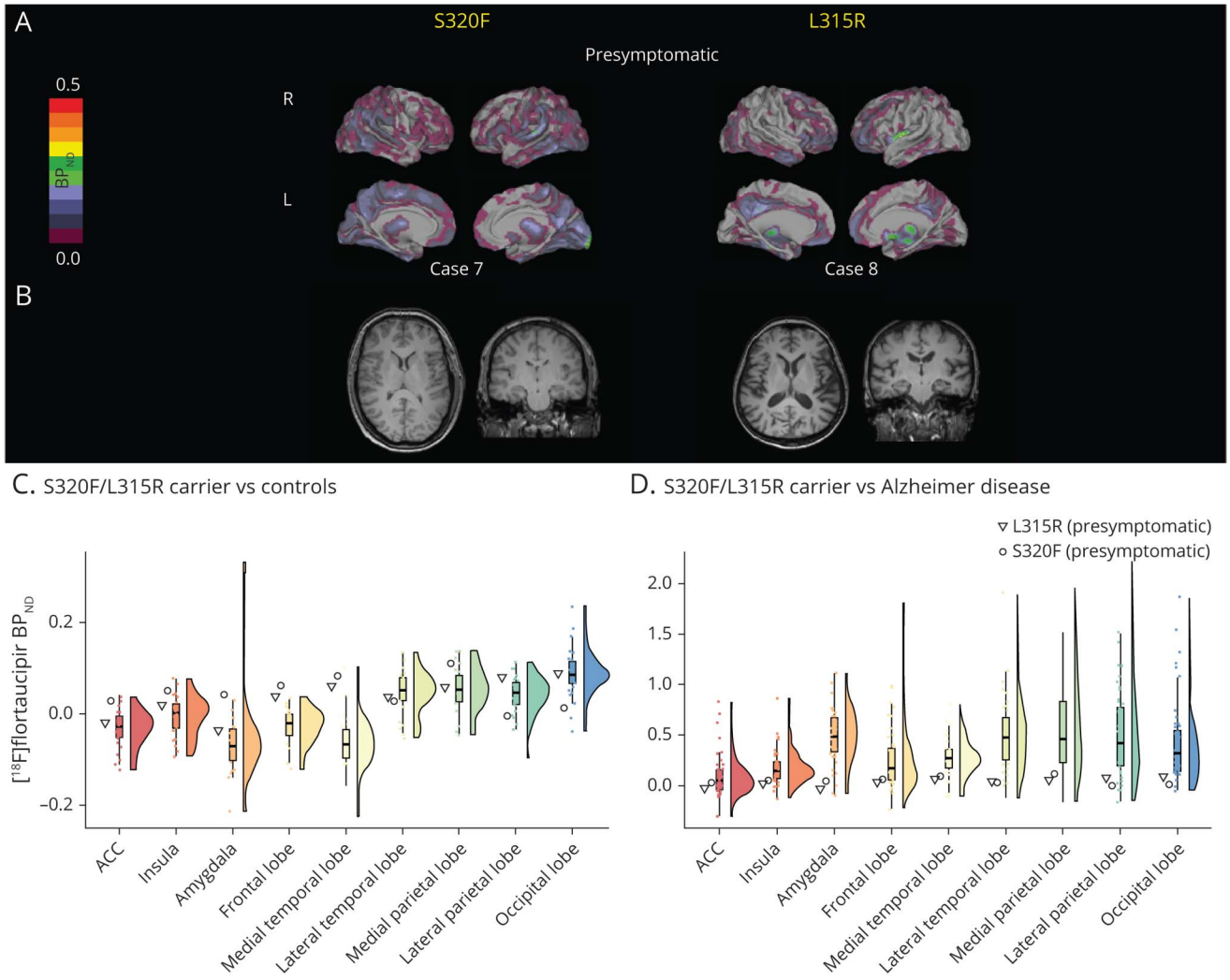


Voxel-wise [$^{18}$F]flortaucipir parametric $BP_{ND}$ images (A), T1-weighted MRI (B), and regional [$^{18}$F]flortaucipir $BP_{ND}$ (C, D) values of the presymptomatic S320F, L315R mutation carriers. (C, D) Presymptomatic S320F, L315R mutation carriers (displayed individually) vs controls (C) and vs patients with Alzheimer disease (D, both displayed as the average of the group). ACC = anterior cingulate cortex.

Microscopically, there was mild gliosis and spongiosis of layer II of the frontal cortex and cingulate gyrus. There was a slight increase in the number of glia cells in the white matter. All other cortical regions, basal ganglia, and hippocampus showed no gliosis or spongiosis.

Tissue immunohistochemistry with tau showed a small to moderate number of tau-immunoreactive positive neurons and some threads in a subset of regions (Figure 5, A–J). Tau burden was most severe in the hippocampus, followed by the temporal cortex and the frontoparietal cortex. In the hippocampus, a moderate number of tau-immunoreactive positive neurons and additional Pick body–like inclusions were found, particularly in the subiculum and CA1, and a small number in the dentate gyrus. The right hippocampus was more severely affected than the left hippocampus, where only sporadic inclusions were found in these areas, in line with asymmetry in brain atrophy on MRI. The transentorhinal cortex was also moderately affected by neuronal tau-immunoreactive inclusions and threads, which were Gallyas negative. The temporal pole showed a few ramified astrocytes, some Pick body–like inclusions (max 9 at 20× objective), and a few threads. The frontal cortex showed the same type of inclusions, but less abundant than in the temporal pole (max 2 at 20× objective). Sporadic tau inclusions were also found in the inferior parietal lobule (max 2–3 at 20× objective), limbic areas (amygdala, anterior cingulate gyrus), and basal ganglia (max 2 inclusions at 20× objective in all regions), while they were absent in the occipital cortex. These inclusions also stained positively for 3R tau isoform, but not for 4R tau. Astrocytic inclusions were not stained positively with either 3R or 4R tau antibodies.

In all cortical regions, basal ganglia, hippocampus, brainstem, and cerebellum, there were several perivascular CD3-positive

**Figure 4** Voxel-wise [$^{18}$F]Flortaucipir Parametric Binding Potential ($BP_{ND}$) Images, T1 -Weighted MRI, and Regional [$^{18}$F] Flortaucipir $BP_{ND}$ Values of the Symptomatic G272V Mutation Carrier

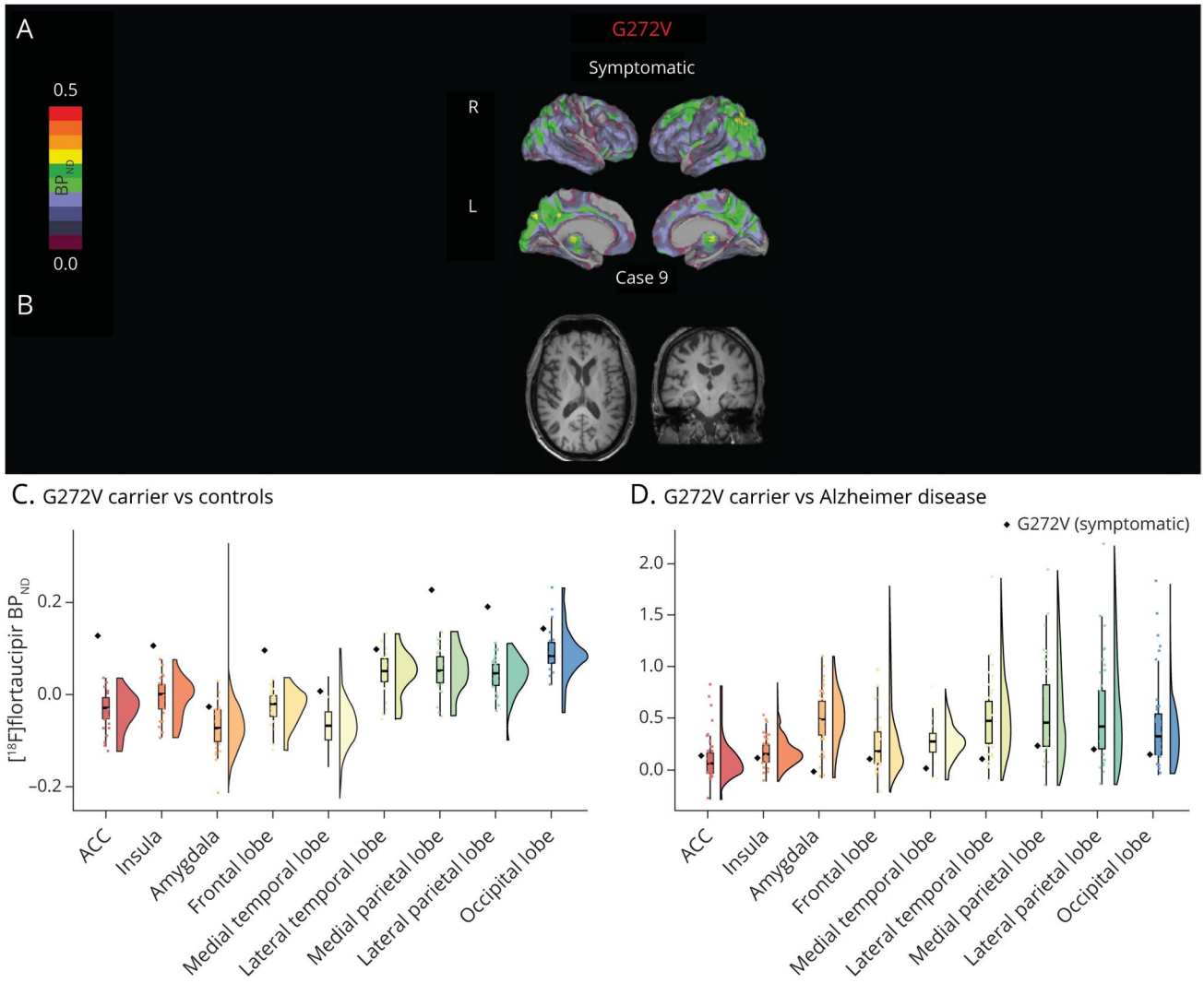


Voxel-wise [$^{18}$F]flortaucipir parametric $BP_{ND}$ images (A), T1-weighted MRI (B), and regional [$^{18}$F]flortaucipir $BP_{ND}$ (C, D) values of the symptomatic G272V mutation carrier. (C, D) Symptomatic G272V mutation carrier (displayed individually) vs controls (C) and vs patients with Alzheimer disease (D, both displayed as the average of the group). ACC = anterior cingulate cortex.

lymphocytic deposits with intraparenchymal infiltrates. Staining with HLA-DR showed severe immune activation of microglia and other myeloid cells around the vasculature and in the brain parenchyma. There was no apparent relationship between this diffuse immune activation, present throughout the entire brain, and the distribution of tau-immunoreactive inclusions. These findings of immune activation and infiltration (Figure 5, G–I) were compatible with a concurrent diagnosis of (autoimmune) encephalitis. There were no signs of a viral or bacterial encephalitis.

## Differential Diagnosis of (Autoimmune) Encephalitis

Because the neuropathologic diagnosis of (auto)immune encephalitis was unexpected, we retrospectively reviewed the clinical data, where there were no seizures or (sub)acute changes in behavior or cognition, apart from the paroxetine-induced manic period. Additional CSF collected for research purposes was evaluated and showed, 2 years before diagnosis, $24 \times 10^6$/L leukocytes (normal $<5 \times 10^6$/L), of which $22 \times 10^6$/L were monocytes, in hindsight suggestive of a viral infection, (autoimmune) encephalitis, or drug induced. However, there were no clinical signs of meningitis or encephalitis or T2/fluid-attenuated inversion recovery abnormalities on MRI that would be suggestive for an autoimmune encephalitis and no drug use associated with pleocytosis at the time of CSF analysis. PCR for neurotrophic viruses and routine diagnostic testing for immune-mediated encephalitis with immunohistochemistry were negative. Leukocytes decreased over time and CSF showed a mild pleocytosis of $9 \times 10^6$/L ($8 \times 10^6$ monocytes) at time of diagnosis.

**Figure 5** Neuropathologic Findings in the Symptomatic G272V Carrier With Early Tauopathy and Concurrent (Auto)immune Encephalitis

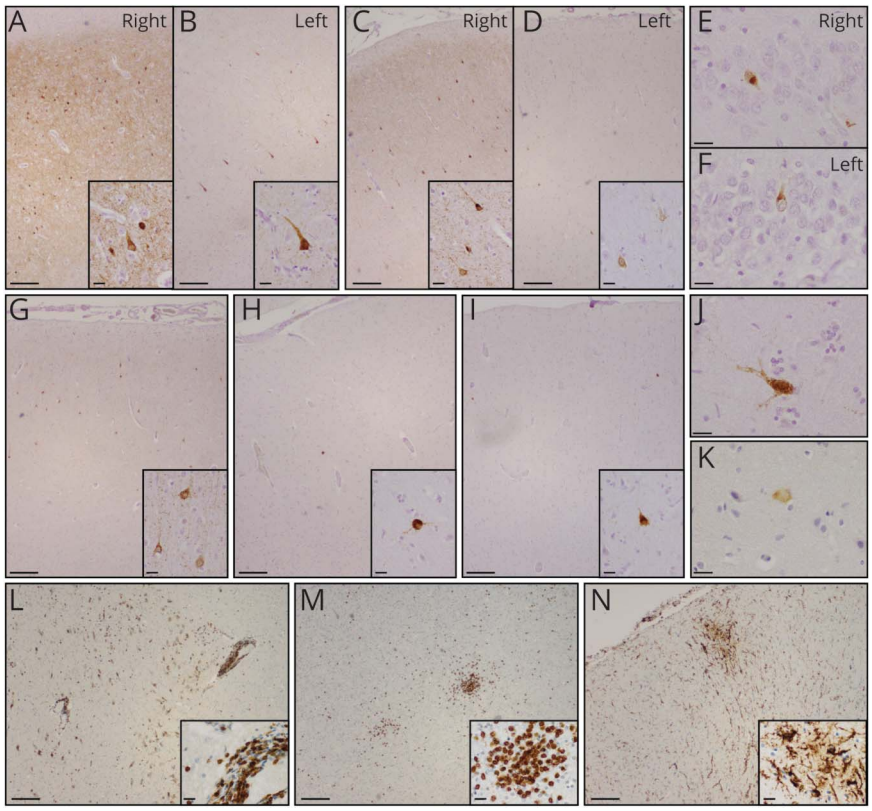


Neuropathologic examination of the symptomatic G272V carrier showed findings consistent with an early tauopathy: moderate amounts of tau-immunoreactive neuronal inclusions and threads in the hippocampus and parahippocampal structures, specifically in the subiculum (A, B), transentorhinal cortex (C, D), and to a lesser extent in the dentate gyrus (E, F); these neuropathologic findings were asymmetrical with greater involvement of the right hippocampus compared to the left hippocampus. Other brain regions, sampled exclusively in the left hemisphere, showed mild gliosis and spongiosis of the upper cortical layers, with moderate amounts of tau-immunoreactive neurons in the temporal cortex (G), fewer tau-immunoreactive neurons in the frontal cortex (H), in the parietal cortex (I), and in limbic and paralimbic areas, such as the amygdala (J) and the insular cortex (K). In addition, neuropathologic findings indicative of a concurrent (auto)immune encephalitis were observed in all examined brain regions, with no apparent relationship to the distribution of tau inclusions: perivascular CD3-positive lymphocytic cuffing with infiltration in the adjacent brain parenchyma in the substantia nigra (L); CD3-positive lymphocytic infiltrates in the brain parenchyma in the cingulate gyrus (M); HLA-DR-positive patchy clustering of activated microglia and myeloid cells in the parahippocampal gyrus (N). Scale bar in large images A–D, G–I, L–N = 200 μm. Scale bar in small images A–D, G–I, L–N, and in images E, F and J, K = 20 μm.

### Regional $R_1$ in (Pre)Symptomatic *MAPT* Mutation Carriers

Figure 6 shows regional values of [$^{18}$F]flortaucipir $R_1$ in (pre)symptomatic *MAPT* mutation carriers compared to average of controls (red boxplots) and patients with AD (blue boxplots). The symptomatic P301L patient showed lower regional $R_1$ values in the ACC, frontal, and lateral temporal lobe, when compared to control values (Figure 6). [$^{18}$F]Flortaucipir $R_1$ values in the G272V patient were elevated in all regions compared to both controls and patients with AD, with exception of the ACC and medial temporal lobe (Figure 6). Regional $R_1$ values of the remaining presymptomatic P301L, R406W, and S320F and symptomatic R406W carriers corresponded to the regional values of both controls and patients with AD, with the exception of the medial temporal lobe (Figure 6).

### [$^{18}$F]Flortaucipir SUVr

To allow comparison of $BP_{ND}$ with SUVr, we show in eFigures 1–4 (data available from Dryad, doi.org/10.5061/dryad.3tx95x6g1) the voxel-wise [$^{18}$F]flortaucipir SUVr images (A) and regional [$^{18}$F]flortaucipir SUVr values (C, D) in (pre)symptomatic mutation carriers vs controls (C) and patients with AD (D) as a reference group. The results were overall comparable between methods.

### Clinical Follow-up After 1 Year

Five out of 6 presymptomatic carriers did not show clinical decline at follow-up after 1 year. One P301L carrier (case 2) showed clinical decline and conversion to symptomatic bvFTD at the follow-up visit after the [$^{18}$F]flortaucipir PET, which consisted of a cognitive assessment (eTable 1, data available from Dryad, doi.org/10.5061/dryad.3tx95x6g1) and MRI (data not shown). At time of [$^{18}$F]flortaucipir PET scan, this carrier did not meet clinical criteria, but did show mild cognitive and behavioral impairment.

## Discussion

Using dynamic [$^{18}$F]flortaucipir PET scanning, we quantified tau burden and examined regional distributions across a variety of *MAPT* mutations in presymptomatic and symptomatic carriers. We found elevated [$^{18}$F]flortaucipir binding compared to controls in both presymptomatic and symptomatic *MAPT* mutation carriers, which was most pronounced in the symptomatic and presymptomatic R406W *MAPT* mutation carriers with a combined 3R/4R tau aggregation.

The (pre)symptomatic R406W carriers showed increased tau binding in the amygdala, temporal lobe, and frontoparietal

**Figure 6** Regional [$^{18}$F]Flortaucipir $R_1$ Values of the (Pre)symptomatic Mutation Carriers vs Controls and Patients With Alzheimer Disease (AD)

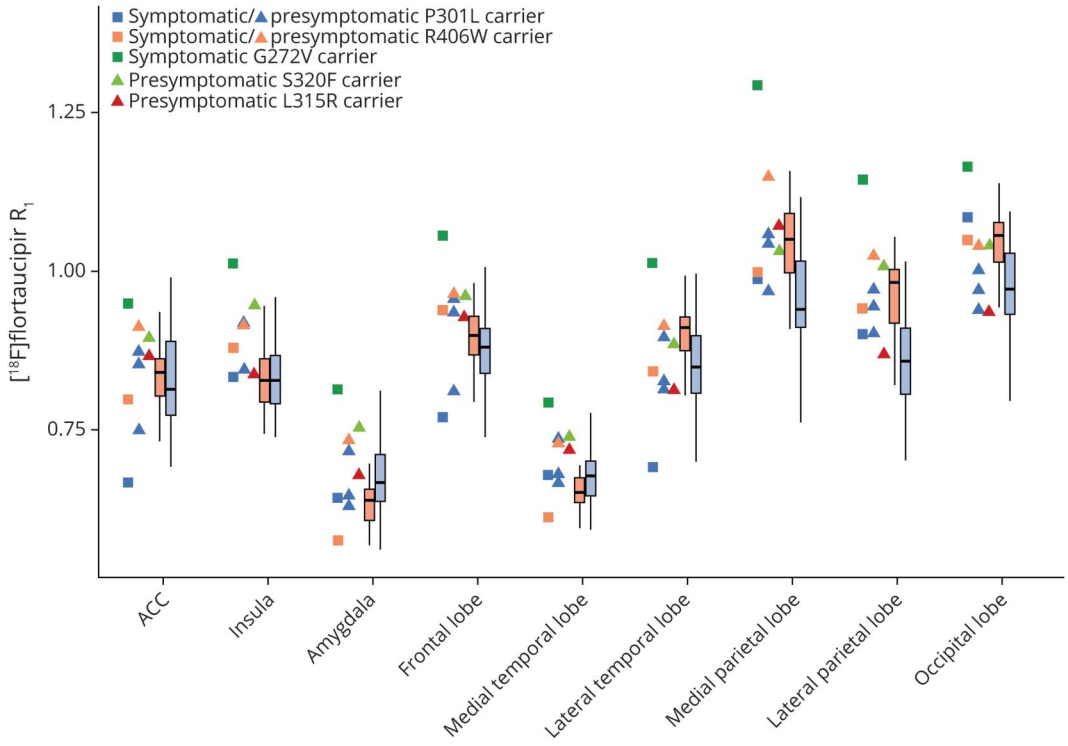


Symptomatic mutation carriers (squares) and presymptomatic carriers (triangles) (displayed individually and color coded per mutation) vs controls (red) and vs patients with AD (blue, both displayed as the average of the group). ACC = anterior cingulate cortex.

regions, which is in line with previous studies in (pre)symptomatic R406W carriers showing frontal and temporal tau with relative sparing of the posterior cortical areas.[7-9] The high binding in the R406W carriers is not surprising as this *MAPT* mutation consists of 3R and 4R tau, similar to those in AD.[3,23] [$^{18}$F]Flortaucipir binds with high affinity to AD tau[4,5] and in vivo [$^{18}$F]flortaucipir retention is strongly associated with postmortem AD neurofibrillary tangle pathology,[7,24,25] indicating that [$^{18}$F]flortaucipir is a reliable method for measuring combinations of 3R/4R PHFs of tau.

Notably, we also observed higher [$^{18}$F]flortaucipir binding in the P301L mutation carriers, a condition typically associated with 4R tau.[26] Two carriers (one presymptomatic, one symptomatic) showed tau binding in the frontal lobe, insula, and parietal lobe, with additional tau binding in the inferior temporal lobe of the symptomatic P301L carrier. This is in line with previous studies showing inconsistent results in P301L carriers[8,9,27] and other 4R tauopathies such as progressive supranuclear palsy,[28-34] varying from low to high binding in individual cases. Variations in tau uptake patterns may be explained by the presence of concomitant amyloid pathology[9] or off-target binding.[28,31-33] Furthermore, in vitro tau has not been associated with postmortem [$^{18}$F]flortaucipir uptake patterns in P301L carriers.[27] Taken together, the evidence that [$^{18}$F]flortaucipir retention is caused by binding to 4R tau is inconclusive.

The presymptomatic S320F and L315R mutation carriers showed low tau binding not exceeding the range observed in controls. Although neuropathologic case studies have shown a specific combination of 3R and 4R tau (one 3R band missing), this is different from AD, which probably explains its low affinity. In addition, these cases were presymptomatic, therefore these carriers may harbor amounts of tau below the detection threshold of tau PET. Our observation of subtly higher frontal tau uptake in the presymptomatic L315R mutation carrier >70 years old possibly represents the first preclinical sign of tau pathology. As incomplete penetrance has been described in L315R families,[35] tau PET uptake may highly depend on disease severity, as previous *MAPT* mutation carrier studies showed an increase in tau with advanced disease stage,[9,11] in correspondence with results found across the AD spectrum.[36,37]

The symptomatic G272V patient exhibited a widespread higher cortical tau binding, relatively sparing the temporal lobe. The gradient of [$^{18}$F]flortaucipir binding did not correspond with postmortem 3R tau, as tracer uptake was most pronounced frontoparietal with sparing of the temporal lobe, while at neuropathologic examination tau-immunoreactive inclusions were most pronounced, although still mild, in the temporal cortex and relatively sparse in frontoparietal lobes. However, the neuropathologic findings were indicative for an

encephalitis and the increased [$^{18}$F]flortaucipir uptake may be the result of binding to nonspecific targets related to neuroinflammation, such as microglial activation,[38] gliosis, or vascular permeability differences.[39,40] In addition, virtually all regions showed higher rCBF vs both controls and patients with AD, which is in line with reported hyperperfusion/hypermetabolism in encephalitis.[41,42]

It is unclear whether this patient had 2 rare disorders or the *MAPT* mutation triggered an (auto)immune response. There is no clear evidence in the literature to support the latter hypothesis, and none of the other G272V brain donors in our Rotterdam FTD cohort (n = 5, data not shown) showed similar features of diffuse abundant perivascular lymphocytes and intraparenchymal infiltrates. Although the role of a chronic neuroinflammatory response is increasingly recognized in FTD,[43] elevated leukocyte levels in the CSF have not been observed in our FTD-RisC cohort in the presymptomatic phase or around conversion to symptomatic phases, nor has this been described by other research groups in the literature. Thus, these findings probably fall outside the clinicopathologic manifestations of FTLD and are suggestive of a concurrent diagnosis of encephalitis.

Increasing evidence is available on identifying neuroimaging biomarkers for genetic FTD in an early phase. For example, recent work showed anterior cingulate abnormalities on both MRI and FDG-PET already in presymptomatic *MAPT* mutation carriers.[44] However, information on combined in vivo and postmortem pathologic disease staging in *MAPT* carriers for tau specifically is limited, due to the low occurrence of presymptomatic or early symptomatic *MAPT* carriers in clinical and research settings, especially with regard to neuropathologic data. The combination of [$^{18}$F]flortaucipir, rCBF, and neuropathologic data in presymptomatic and early symptomatic phases is unique and may help clarify spread of tau accumulation in *MAPT* mutation carriers. [$^{18}$F]Flortaucipir uptake in R406W carriers is most robust. Although based on cross-sectional data, our study and previous [$^{18}$F]flortaucipir PET studies[7,9] in R406W carriers suggest that tau accumulation may start in the medial temporal lobe in the presymptomatic phase and finally spread into the frontal and parietal lobe, as observed in our symptomatic R406W carrier. The P301L carriers showed a more frontoparietal [$^{18}$F]flortaucipir binding pattern in the presymptomatic phase with involvement of temporal lobe only in the symptomatic phase. This should be interpreted with caution because P301L carriers, in line with the literature,[8] probably lack association between advancing disease stage and tau uptake, as we found minimal tau binding in the presymptomatic P301L carrier (case 2) who converted to symptomatic phase.

In the early symptomatic G272V carrier, the highest neuropathologic tau load in the right hippocampus corresponded with the region of atrophy on MRI. Only tissue blocks from the left hemisphere were available and showed very little amount of tau pathology, 2 years after onset, with the left frontal and parietal lobe similarly affected. It also must be considered that *MAPT* mutations show a great heterogeneity of pathologic features,[45] and G272V mutations have overall relatively low tau burden compared to other mutations, such as P301L. Possibly, a dynamic [$^{18}$F]flortaucipir PET scan is of additional value to study disease spread, providing an additional measure of rCBF. Previous rCBF dynamic PET studies with inclusion of patients with bvFTD showed a good correlation between rCBF and FDG-PET hypometabolism patterns.[46] Compared to controls, low rCBF in the ACC, lateral temporal, and frontal lobe in the symptomatic P301L patient is largely in correspondence with a previous SPECT study in symptomatic *MAPT* mutation carriers.[22] Interestingly, borderline abnormal low ACC rCBF compared to controls was found in one presymptomatic P301L mutation carrier, confirming the results of a previous study that found glucose hypometabolism in the anterior cingulate of presymptomatic P301L carriers.[44] More longitudinal (dynamic) tau PET studies in presymptomatic and symptomatic carriers in combination with different imaging techniques[47,48] and in-depth neuropathologic data are needed to give a better and more complete overview of pathology spreading in different disease stages and various *MAPT* mutations.

Strengths of this study include the performance of dynamic [$^{18}$F]flortaucipir scans, which allows for simultaneous quantification of measures of both tau load and rCBF in presymptomatic and symptomatic carriers of various *MAPT* mutations and allowed for examining tau pathology/rCBF in a very early phase of the disease.

Limitations include the small number of carriers per mutation, which precluded statistical comparisons. Although the presence of amyloid pathology in *MAPT* carriers could not be ruled out, it is very unlikely given that the majority of the carriers were ~50 years of age (although one *MAPT* carrier was >70 years of age).[49,50] Furthermore, neuropathologic data were available for only one case in this study, which is instrumental to better understand the binding properties of [$^{18}$F]flortaucipir. However, several *MAPT* mutation cases have been described neuropathologically in other studies in combination with in vivo assessment of tau pathology using [$^{18}$F]flortaucipir PET[6,7,27] and show that [$^{18}$F]flortaucipir binds predominantly to combined 3R/4R tauopathies, which could be generalized to our study.

We found subtle increased tau binding in a significant proportion of the presymptomatic *MAPT* mutation carriers, whereas higher magnitude of [$^{18}$F]flortaucipir binding was observed in symptomatic *MAPT* mutation carriers. Furthermore, increased tau load was mainly observed in those (pre) symptomatic mutation carriers with combined 3R/4R tau. Taken together, these findings suggest that [$^{18}$F]flortaucipir PET may be used as an early biomarker in *MAPT* mutation carriers, in particular in a subset of *MAPT* mutation carriers who include mutations that cause 3R/4R tauopathies. Thereby, [$^{18}$F]flortaucipir potentially binds to lower tau

concentrations or nonspecific targets, as we observed mild [$^{18}$F]flortaucipir signal in 3R/4R only *MAPT* mutation carriers. Future longitudinal [$^{18}$F]flortaucipir studies with postmortem confirmation will be essential to capture the complexity and progression of the in vivo findings observed with [$^{18}$F]flortaucipir in (pre)symptomatic *MAPT* mutation carriers.


## Acknowledgment

[$^{18}$F]Flortaucipir PET scans were made possible by Avid Radiopharmaceuticals Inc. The brain tissue and CSF were obtained from The Netherlands Brain Bank (NBB), Netherlands Institute for Neuroscience, Amsterdam. The material has been collected from donors who provided written informed consent for brain autopsy and the use of the material and clinical information for research purposes has been obtained by the NBB. The SCIENCe project receives support from Gieskes Strijbis fonds and Stichting Dioraphte. W.M.v.d.F. holds the Pasman chair. Several authors of this publication are members of the European Reference Network for Rare Neurological Diseases (Project ID No. 739510).

## Study Funding

ZonMw Memorabel grant.


## Disclosure

E.E. Wolters, J.M. Papma, S.C.J. Verfaillie, D. Visser, E. Weltings, C. Groot, E.L. van der Ende, L.A.A. Giannini, H. Tuncel, T. Timmers, R. Boellaard, M. Yaqub, D.M.E. van Assema, D.A. Kuijper, M. Segbers, A.J.M. Rozemuller, A.D. Windhorst, Y.A.L. Pijnenburg, J.C. van Swieten, and R. Ossenkoppele report no disclosures. W.M. van der Flier receives grant support from ZonMw, NWO, EU-FP7, Alzheimer Nederland, CardioVascular Onderzoek Nederland, Stichting Dioraphte, Gieskes-Strijbis Fonds, Boehringer Ingelheim, Piramal Neuroimaging, Roche BV, Janssen Stellar, and Combinostics; all funding is paid to the institution. W.M. van der Flier holds the Pasman chair. B.N.M. van Berckel receives research support from ZonMw, AVID Radiopharmaceuticals, CTMM, and Janssen Pharmaceuticals; is a trainer for Piramal and GE; and receives no personal honoraria. F. Barkhof is an editorial board member of *Brain*, *European Radiology*, *Neurology*, *Multiple Sclerosis Journal*, and *Radiology*; performed consultancy and received personal compensation and honoraria from Bayer-Schering Pharma and Genzyme; received compensation (personal and to institution) and honoraria from Biogen-IDEC, TEVA, Merck-Serono, Novartis, Roche, Synthon BV, and Jansen Research; received payment for development of educational presentations from IXICO and Biogen-IDEC (to institution); is funded by a Dutch MS Society grant, EU-FP7/H2020; and is supported by the NIH Research Biomedical Research Center at University College London Hospital. P. Scheltens has received consultancy/speaker fees (paid to the institution) from Biogen, Novartis Cardiology, Genentech, and AC Immune; and is PI of studies with Vivoryon, EIP Pharma, IONIS, CogRx, AC Immune and Fujifilm/Toyama. H. Seelaar receives research support from ZonMW. Go to Neurology.org/N for full disclosures.


## Publication History

Received by *Neurology* February 17, 2021. Accepted in final form June 7, 2021.


## Appendix Authors

| Name | Location | Contribution |
|---|---|---|
| **Emma E. Wolters, MD, PhD** | Amsterdam UMC, the Netherlands | Designed and conceptualized study, analyzed the data, drafted the manuscript for intellectual content |
| **Janne M. Papma, PhD** | Erasmus MC University Medical Center, Rotterdam, the Netherlands | Designed and conceptualized study, analyzed the data, interpreted the data, revised the manuscript for intellectual content |
| **Sander C.J. Verfaillie, PhD** | Amsterdam UMC, the Netherlands | Interpreted the data, revised the manuscript for intellectual content |
| **Denise Visser, MSc** | Amsterdam UMC, the Netherlands | Major role in the acquisition of data |
| **Emma Weltings, MSc** | Amsterdam UMC, the Netherlands | Major role in the acquisition of data |
| **Colin Groot, PhD** | Amsterdam UMC, the Netherlands | Analyzed the PET data |
| **Emma L. van der Ende, MD** | Erasmus MC University Medical Center, Rotterdam, the Netherlands | Major role in the acquisition of data |
| **Lucia A.A. Giannini, MD** | Erasmus MC University Medical Center, Rotterdam, the Netherlands | Analyzed the neuropathologic data, revised the manuscript for intellectual content. |
| **Hayel Tuncel, MSc** | Amsterdam UMC, the Netherlands | Analyzed the PET data |
| **Tessa Timmers, MD, PhD** | Amsterdam UMC, the Netherlands | Major role in the acquisition of data |
| **Ronald Boellaard, PhD** | Amsterdam UMC, the Netherlands | Revised the manuscript for intellectual content |
| **Maqsood Yaqub, PhD** | Amsterdam UMC, the Netherlands | Analyzed the data, revised the manuscript for intellectual content |
| **Danielle M.E. van Assema, MD, PhD** | Erasmus MC University Medical Center, Rotterdam, the Netherlands | Major role in the acquisition of data, revised the manuscript for intellectual content |
| **Dennis A. Kuijper, MSc** | Erasmus MC University Medical Center, Rotterdam, the Netherlands | Major role in the acquisition of data |
| **Marcel Segbers, MSc** | Erasmus MC University Medical Center, Rotterdam, the Netherlands | Major role in the acquisition of data, revised the manuscript for intellectual content |

## Appendix *(continued)*

| Name | Location | Contribution |
|---|---|---|
| **Annemieke J.M. Rozemuller, MD, PhD** | Amsterdam UMC, the Netherlands | Analyzed the neuropathologic data, revised the manuscript for intellectual content |
| **Frederik Barkhof, MD, PhD** | Amsterdam UMC, the Netherlands; UCL, London, UK | Revised the manuscript for intellectual content |
| **Albert D. Windhorst, PhD** | Amsterdam UMC, the Netherlands | Revised the manuscript for intellectual content |
| **Wiesje M. van der Flier, PhD** | Amsterdam UMC, the Netherlands | Revised the manuscript for intellectual content |
| **Yolande A.L. Pijnenburg, MD, PhD** | Amsterdam UMC, the Netherlands | Revised the manuscript for intellectual content |
| **Philip Scheltens, MD, PhD** | Amsterdam UMC, the Netherlands | Revised the manuscript for intellectual content |
| **Bart N.M. van Berckel, MD, PhD** | Amsterdam UMC, the Netherlands | Designed and conceptualized study, revised the manuscript for intellectual content |
| **John C. van Swieten, MD, PhD** | Erasmus MC University Medical Center, Rotterdam, the Netherlands | Designed and conceptualized study, revised the manuscript for intellectual content |
| **Rik Ossenkoppele, PhD** | Amsterdam UMC, the Netherlands; Lund University, Sweden | Designed and conceptualized study, analyzed the data, interpreted the data, revised the manuscript for intellectual content |
| **Harro Seelaar, MD, PhD** | Erasmus MC University Medical Center, Rotterdam, the Netherlands | Major role in the acquisition of data, interpreted the data, revised the manuscript for intellectual content |

## References


1. Rascovsky K, Hodges JR, Knopman D, et al. Sensitivity of revised diagnostic criteria for the behavioural variant of frontotemporal dementia. *Brain.* 2011;134(pt 9):2456-2477.
2. Gorno-Tempini ML, Hillis AE, Weintraub S, et al. Classification of primary progressive aphasia and its variants. *Neurology.* 2011;76(11):1006-1014.
3. van Swieten J, Spillantini MG. Hereditary frontotemporal dementia caused by tau gene mutations. *Brain Pathol.* 2007;17(1):63-73.
4. Chien DT, Bahri S, Szardenings aK, et al. Early clinical PET imaging results with the novel PHF-tau radioligand [F-18]-T807. *J Alzheimers Dis.* 2013;34(2):457-468.
5. Xia C-F, Arteaga J, Chen G, et al. [F]T807, a novel tau positron emission tomography imaging agent for Alzheimer's disease. *Alzheimer Dement.* 2013;9(6):666-676.
6. Spina S, Schonhaut DR, Boeve BF, et al. Frontotemporal dementia with the V337M MAPT mutation: tau-PET and pathology correlations. *Neurology.* 2017;88(8):758-766.
7. Smith R, Puschmann A, Scholl M, et al. 18F-AV-1451 tau PET imaging correlates strongly with tau neuropathology in MAPT mutation carriers. *Brain.* 2016;139(pt 9):2372-2379.
8. Jones DT, Knopman DS, Graff-Radford J, et al. In vivo F-AV-1451 tau PET signal in MAPT mutation carriers varies by expected tau isoforms. *Neurology.* 2018;90(11):e947-e954.
9. Tsai RM, Bejanin A, Lesman-Segev O, et al. (18)F-flortaucipir (AV-1451) tau PET in frontotemporal dementia syndromes. *Alzheimer Res Ther.* 2019;11(1):13.
10. Ono M, Sahara N, Kumata K, et al. Distinct binding of PET ligands PBB3 and AV-1451 to tau fibril strains in neurodegenerative tauopathies. *Brain.* 2017;140(3):764-780.
11. Convery RS, Jiao J, Clarke MTM, et al. Longitudinal (F)AV-1451 PET imaging in a patient with frontotemporal dementia due to a Q351R MAPT mutation. *J Neurol Neurosurg Psychiatry.* 2020;91(1):106-108.
12. Bevan Jones WR, Cope TE, Passamonti L, et al. [F]AV-1451 PET in behavioral variant frontotemporal dementia due to MAPT mutation. *Ann Clin Transl Neurol.* 2016;3(12):940-947.
13. Bevan-Jones WR, Cope TE, Jones PS, et al. In vivo evidence for pre-symptomatic neuroinflammation in a MAPT mutation carrier. *Ann Clin Transl Neurol.* 2019;6(2):373-378.
14. Dopper EG, Rombouts SA, Jiskoot LC, et al. Structural and functional brain connectivity in presymptomatic familial frontotemporal dementia. *Neurology.* 2014;83(2):e19-e26.
15. Jiskoot LC, Panman JL, Meeter LH, et al. Longitudinal multimodal MRI as prognostic and diagnostic biomarker in presymptomatic familial frontotemporal dementia. *Brain.* 2019;142(1):193-208.
16. Wolters EE, van de Beek M, Ossenkoppele R, et al. Tau PET and relative cerebral blood flow in dementia with Lewy bodies: a PET study. *Neuroimage Clin.* 2020;28:102504.
17. Slot RER, Verfaillie SCJ, Overbeek JM, et al. Subjective Cognitive Impairment Cohort (SCIENCe): study design and first results. *Alzheimers Res Ther.* 2018;10(1):76.
18. Hammers A, Allom R, Koepp MJ, et al. Three-dimensional maximum probability atlas of the human brain, with particular reference to the temporal lobe. *Hum Brain Mapp.* 2003;19(4):224-247.
19. Golla SS, Wolters EE, Timmers T, et al. Parametric methods for [18F] flortaucipir PET. *J Cereb Blood Flow Metab.* 2020;40(2):365-373.
20. Peretti DE, Vallez Garcia D, Reesink FE, et al. Relative cerebral flow from dynamic PIB scans as an alternative for FDG scans in Alzheimer's disease PET studies. *PLoS One.* 2019;14(1):e0211000.
21. Mutsaerts H, Mirza SS, Petr J, et al. Cerebral perfusion changes in presymptomatic genetic frontotemporal dementia: a GENFI study. *Brain.* 2019;142(4):1108-1120.
22. Seelaar H, Papma JM, Garraux G, et al. Brain perfusion patterns in familial frontotemporal lobar degeneration. *Neurology.* 2011;77(4):384-392.
23. Hutton M, Lendon CL, Rizzu P, et al. Association of missense and 5'-splice-site mutations in tau with the inherited dementia FTDP-17. *Nature.* 1998;393(6686):702-705.
24. Lowe VJ, Lundt ES, Albertson SM, et al. Tau-positron emission tomography correlates with neuropathology findings. *Alzheimer Dement.* 2020;16(3):561-571.
25. Fleisher AS, Pontecorvo MJ, Devous MD Sr, et al. Positron emission tomography imaging with [18F]flortaucipir and postmortem assessment of Alzheimer disease neuropathologic changes. *JAMA Neurol.* 2020;77(7):829-839.
26. Spillantini MG, Murrell JR, Goedert M, Farlow MR, Klug A, Ghetti B. Mutation in the tau gene in familial multiple system tauopathy with presenile dementia. *Proc Natl Acad Sci USA.* 1998;95(13):7737-7741.
27. Marquie M, Normandin MD, Meltzer AC, et al. Pathological correlations of [F-18]-AV-1451 imaging in non-Alzheimer tauopathies. *Ann Neurol.* 2017;81(1):117-128.
28. Smith R, Schain M, Nilsson C, et al. Increased basal ganglia binding of F-AV-1451 in patients with progressive supranuclear palsy. *Mov Disord.* 2017;32(1):108-114.
29. Hammes J, Bischof GN, Giehl K, et al. Elevated in vivo [18F]-AV-1451 uptake in a patient with progressive supranuclear palsy. *Mov Disord.* 2017;32(1):170-171.
30. Whitwell JL, Lowe VJ, Tosakulwong N, et al. [18 F]AV-1451 tau positron emission tomography in progressive supranuclear palsy. *Mov Disord.* 2017;32(1):124-133.
31. Passamonti L, Vazquez Rodriguez P, Hong YT, et al. 18F-AV-1451 positron emission tomography in Alzheimer's disease and progressive supranuclear palsy. *Brain.* 2017;140(3):781-791.
32. Schonhaut DR, McMillan CT, Spina S, et al. $^{18}$F-flortaucipir tau positron emission tomography distinguishes established progressive supranuclear palsy from controls and Parkinson disease: a multicenter study. *Ann Neurol.* 2017;82(4):622-634.
33. Cho H, Choi JY, Hwang MS, et al. Subcortical F-AV-1451 binding patterns in progressive supranuclear palsy. *Mov Disord.* 2017;32(1):134-140.
34. Coakeley S, Cho SS, Koshimori Y, et al. Positron emission tomography imaging of tau pathology in progressive supranuclear palsy. *J Cereb Blood Flow Metab.* 2017;37(9):3150-3160.
35. van Herpen E, Rosso SM, Serverijnen LA, et al. Variable phenotypic expression and extensive tau pathology in two families with the novel tau mutation L315R. *Ann Neurol.* 2003;54(5):573-581.
36. Ossenkoppele R, Rabinovici GD, Smith R, et al. Discriminative accuracy of [18F] flortaucipir positron emission tomography for Alzheimer disease vs other neurodegenerative disorders. *JAMA.* 2018;320(11):1151-1162.
37. Cho H, Choi JY, Lee HS, et al. Progressive tau accumulation in Alzheimer disease: 2-year follow-up study. *J Nucl Med.* 2019;60(11):1611-1621.
38. Bevan-Jones WR, Cope TE, Jones PS, et al. Neuroinflammation and protein aggregation co-localize across the frontotemporal dementia spectrum. *Brain.* 2020;143(3):1010-1026.
39. Cho H, Seo SW, Choi JY, et al. Predominant subcortical accumulation of F-flortaucipir binding in behavioral variant frontotemporal dementia. *Neurobiol Aging.* 2018;66:112-121.
40. Lockhart SN, Ayakta N, Winer JR, La Joie R, Rabinovici GD, Jagust WJ. Elevated F-AV-1451 PET tracer uptake detected in incidental imaging findings. *Neurology.* 2017;88(11):1095-1097.
41. Tripathi M, Tripathi M, Roy SG, et al. Metabolic topography of autoimmune non-paraneoplastic encephalitis. *Neuroradiology.* 2018;60(2):189-198.
42. Sachs JR, Zapadka ME, Popli GS, Burdette JH. Arterial spin labeling perfusion imaging demonstrates cerebral hyperperfusion in anti-NMDAR encephalitis. *Radiol Case Rep.* 2017;12(4):833-837.
43. Bright F, Werry EL, Dobson-Stone C, et al. Neuroinflammation in frontotemporal dementia. *Nat Rev Neurol.* 2019;15(9):540-555.

44. Clarke MTM, St-Onge F, Beauregard JM, et al. Early anterior cingulate involvement is seen in presymptomatic MAPT P301L mutation carriers. *Alzheimers Res Ther.* 2021; 13(9):42.
45. Ghetti B, Oblak AL, Boeve BF, Johnson KA, Dickerson BC, Goedert M. Invited review: frontotemporal dementia caused by microtubule-associated protein tau gene (MAPT) mutations: a chameleon for neuropathology and neuroimaging. *Neuropathol Appl Neurobiol.* 2015;41(1):24-46.
46. Asghar M, Hinz R, Herholz K, Carter SF. Dual-phase [18F]florbetapir in frontotemporal dementia. *Eur J Nucl Med Mol Imaging.* 2019;46(2):304-311.
47. Dopper EG, Chalos V, Ghariq E, et al. Cerebral blood flow in presymptomatic MAPT and GRN mutation carriers: a longitudinal arterial spin labeling study. *Neuroimage Clin.* 2016;12:460-465.
48. Chen Q, Boeve BF, Senjem M, et al. Rates of lobar atrophy in asymptomatic MAPT mutation carriers. *Alzheimers Dement.* 2019;5:338-346.
49. Ossenkoppele R, Jansen WJ, Rabinovici GD, et al. Prevalence of amyloid PET positivity in dementia syndromes. *JAMA.* 2015;313(19):1939-1949.
50. Jansen WJ, Ossenkoppele R, Knol DL, et al. Prevalence of cerebral amyloid pathology in persons without dementia. *JAMA.* 2015;313(19):1924-1938.